Load Snapshot Based Nonlinear-Input Model Order Reduction of a Thermal Human Tissue Model

Onkar Jadhav[1], Evgenii Rudnyi[3], and Tamara Bechtold[2,1]

Abstract Electrically active implants are extremely important today as a part of modern advanced medical technologies. Enhancing or replacing certain functions of a specific tissue or organ in the human body is their distinct clinical role. In this work, we present a compact thermal model of a miniaturized thermoelectric generator embedded into human tissue structure, for powering electrically active implants. Heat generation by tissue perfusion is modeled as a temperature dependent effect; thus resulting in a nonlinear-input model. We apply mathematical methods of model order reduction to create a compact but highly accurate reduced order thermal model. To overcome the nonlinear-input problem, we linearize the load vector by snapshotting it prior to applying model order reduction. The reduced order linearized model is compared to the full scale model with nonlinear input.

1 Introduction

Implantable medical devices are used to provide medical treatments and support the diagnosis [1]. Medical technology, which improves the efficiency of necessary medical treatments, is therefore gaining more concern. The need for developing implantable medical devices for regeneration of bone and cartilage, deep brain stimulation or cardiac pacing is rapidly increasing. Currently, the electrical energy for implantable biomedical devices is provided by integrated batteries. However, batteries suffer from limited energy storage capacity, limited lifetime, chemical side

Onkar Jadhav, Tamara Bechtold, Cheng Dong Yuan
Institute of Electronic Appliances and Circuits, University of Rostock, Rostock, Germany

Evgenii Rudnyi
CADFEM GmbH, Germany

Tamara Bechtold, Cheng Dong Yuan
Department of Engineering, Jade University of Applied Sciences, Wilhelmshaven, Germany
e-mail: tamara.bechtold@jade-hs.de

effects, and large size [2]. Furthermore, repeated surgery is required to replace batteries.

As human body is a bountiful source of thermal energy, harvesting this energy to power biomedical implants will increase their lifetime and will provide more comfort and safety than conventional devices [3]. A novel miniaturized thermoelectric generator (TEG) embedded into a human body will employ the Seebeck effect to convert thermal into electrical energy and thus power the medical implants [4, 5]. It will utilize the temperature difference across the tissue structure, as human body maintains the core temperature of 37 C and the skin surface temperature amounts to approximately 22 C to 30 C. Core temperature is maintained by metabolic heat generation, an intra-cellular bio-chemical process [6]. The heat is transferred throughout the body by blood perfusion, a mechanism which can be modeled by local temperature dependent heat generation rate. This temperature dependent heat generation rate represents the nonlinear input into the thermal model. To enable efficient simulations, we apply mathematical model order reduction (MOR) [7], which was shown to provide accurate compact thermal models for linear systems [8]. In the approach presented here, the snapshot based linearization of a temperature dependent heat generation rate is performed and the reduced model is obtained for this linearized input.

2 Case Study - Human TEG

In this work, we present the model of a TEG embedded into a simplified three layer tissue structure. Figure 1 shows schematically the TEG embedded into a fat layer where, maximum temperature difference can be obtained as presented in [9].

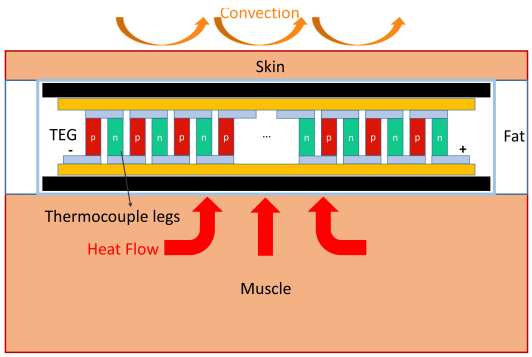

Fig. 1 Schematic of a thermoelectric generator embedded in the fat layer.

A simplified cake-like model (See Fig. 2) composed of muscle, fat and skin tissues has been built for this case study. Thermal material properties of each tissue layer are given in Table 1.

Table 1 Thermal material properties of tissues

material property	muscle	fat	skin	blood
Density r [kg/m^3]	1090.4	911	1109	1049.75
Specific heat capacity c_p [J/kg/K]	3421.2	2348.3	3390.5	3617
Thermal conductivity k [W/m/K]	0.4949	0.2115	0.3722	0.5168
Perfusion rate w [1/s]	0.0004	0.0003	0.0012	0.1749

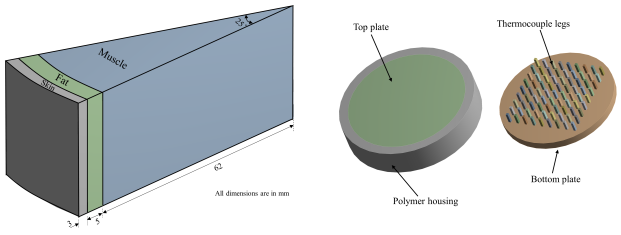

Fig. 2 Human tissue cake-like model with muscle, fat and skin layers (left). TEG model with cylindrical housing and thermocouple legs array inside the fat layer (right).

The heat conduction in the tissue is given by the bioheat equation of Pennes [10]:

$$r c_p \frac{\P T}{\P t} = \tilde{N} k \tilde{N} T + Q_b + Q_m, \tag{1}$$

where, $Q_b = r_b c_b w(T_a \quad T(\mathbf{r}))$ and Q_m are perfusion and metabolic heat generation rates, respectively. r, c_p, k are the density, specific heat and thermal conductivity of the three tissue types. r_b, c_b denote the thermal properties of blood and w is a tissue-dependent measure of perfusion. $T(\mathbf{r})$ is the resulting temperature distribution and $T_a = 37$ C, is the temperature of arterial blood. Furthermore, the heat dissipated from the skin surface is modeled by convection boundary condition:

$$q_? = h \ (T(t) \quad T_{amb}), \tag{2}$$

where, $q_?$ is the heat flux normal to the boundary skin surface, T_{amb} is the ambient temperature and h is the heat transfer coefficient in W/m^2/K. The TEG itself consists of two metallic discs (diameter 13 mm, height 0.9 mm) and an array of 9 9 thermocouple legs of Bismuth-telluride ($k = 1.35$ W/m/K, $a = 200$ V/K, $r_{el} = 10$ Wm) in between. It is enclosed by a polymer housing with low thermal conductivity ($k = 0.25$ W/m/K).

Note that, for this MOR case study, we consider purely thermal model of the TEG. Furthermore, we perform the transient thermal simulation, to follow the change of the heat transfer coefficient from $h = 20$ W/m^2/K to $h = 5$ W/m^2/K at ambient temperature of 15 C.

3 Model Order Reduction

The numerical analysis of the TEG implanted thermal tissue model is carried out by means of finite element method. The model (1) can be spatially discretized and represented as the following set of ordinary differential equations:

$$\sum_{n} \begin{cases} E\ \dot{T}(t) = A\ T(t) + \underbrace{B\ u(T(t))}_{Q} \\ y(t) = C\ T(t), \end{cases} \tag{3}$$

where, $A, E \in R^{n\ n}$ are the global heat conductivity and heat capacity matrices, $B \in R^{n\ m}$ is the load vector (matrix) and $C \in R^{p\ n}$ is the output vector (matrix). $T(t) \in R^{n}$ is the vector of unknown temperatures, n is the dimension of the system and m and p are the number of inputs and user defined outputs, respectively. Note that, Q is the load vector given as,

$$Q = r_b c_b w_b (T_a \quad T(\mathbf{r}, t)) + Q_m \tag{4}$$

which presents on the right hand side of the system (3).

To construct the reduced order model, we apply Krylov subspace based MOR. Different from the approach in [11], where, the time consuming singular value decomposition (SVD) of the thermal load snapshots is performed, in our approach, the load snapshots, obtained at discrete time intervals, are weighted to obtain a single linearized load for the model to be reduced.

Equation 3 with such linearized load vector can be represented as:

$$\sum_{n} \begin{cases} E\ \dot{T}(t) = A\ T(t) + \bar{Q} \\ y(t) = C\ T(t), \end{cases} \tag{5}$$

The exact generation of linearized load vector will be explain in the section 4.

After applying the block Arnoldi algorithm from [12] to (5), we obtain the reduced model as follows:

$$\sum_{r} \begin{cases} E_r\ \dot{z}(t) = A_r\ z(t) + \bar{Q}_r \\ y_r(t) = C_r\ z(t), \end{cases} \tag{6}$$

where, $E_r = V^T E V, A_r = V^T A V, \bar{Q}_r = V^T \bar{Q}, C_r = CV$ and $V \in R^{n\ r}$ is the projection matrix. Here, a generalized variable $z(t)$ can be seen as a projection of n-dimensional temperature vector to r-dimensional subspace, subjected to some some error e:

$$T(t) = V\ z(t) + e, z(t) \in R^{r}, r \quad n \tag{7}$$

and $y_r(t) = C_r\ z(t)$ is the linear combination of the reduced states, which corresponds to the chosen outputs $y(t)$ in (5).

In the Krylov subspace based moment matching approach [12], the subspace V is found in such a way that r moments (Taylor coefficients) of the transfer function

of (5), defined as:

$$H(s) = C(sE - A)^{-1}\bar{Q} \tag{8}$$

are preserved within a reduced model with respect to the Laplace variable s around some apriori chosen value s_0. For example, the Taylor expansion of (8) around $s_0 = 0$ reads:

$$\begin{aligned} H(s) &= H(0) + \frac{\partial H}{\partial s}(0)\, s + \frac{1}{2!}\frac{\partial^2 H}{\partial s^2}(0)\, s^2 + \ldots \\ &= \sum_{j=0}^{\infty} \underbrace{C(A^{-1}E)^j A^{-1}\bar{Q}}_{m_i,\quad i=1,\ldots,r} s^j \end{aligned} \tag{9}$$

The expansion coefficients m_i are called moments of the transfer function. When V is defined as an orthonormal bases of the following Krylov subspace:

$$\begin{aligned} colspan\{V\} &= \mathcal{K}_r\{A^{-1}E, A^{-1}\bar{Q}\} \\ &= \{A^{-1}\bar{Q}, (A^{-1}E)A^{-1}\bar{Q}, \ldots, (A^{-1}E)^r A^{-1}\bar{Q}\} \end{aligned} \tag{10}$$

one obtains a reduced order r model (6) by projecting (5) onto V. The transfer function of (6) is defined as:

$$H_r(s) = C_r(sE_r - A_r)^{-1}\bar{Q}_r \tag{11}$$

and its Taylor expansion around $s_0 = 0$ reads:

$$\begin{aligned} H_r(s) &= H_r(0) + \frac{\partial H_r}{\partial s}(0)\, s + \frac{1}{2!}\frac{\partial^2 H_r}{\partial s^2}(0)\, s^2 + \ldots \\ &= \sum_{j=0}^{\infty} \underbrace{C_r(A_r^{-1}E_r)^j A_r^{-1}\bar{Q}_r}_{m_i^{(r)},\quad i=1,\ldots,r} s^j \end{aligned} \tag{12}$$

The property of the Krylov subspace (10) is such that the first r moments m_i and $m_i^{(r)}$ of (9) and (12) are matched and hence, the reduced model is an accurate approximation of the full scale model.

4 Generation of Linearized Load Vector

The nonlinear perfusion heat generation Q depends on the spatially varying temperature distribution across the tissue structure $T(r)$, as given by (4). The finite element method (FEM) discretizes the computational domain into n nodes and e finite elements.

From (4), the heat generation per finite element in each tissue layer can be written as:

$$Q_e = r_b c_b w_b (T_a - T_e) + Q_m, \tag{13}$$

where, T_e is the average temperature of the finite element e. Furthermore, we construct a snapshot matrix $X \in R^{e \times s}$ at s points in time (t_i), whose columns are comprised of elemental heat generation vectors, q_i:

$$X = [q_1 \quad q_2 \quad q_3 \quad \dots \quad q_n]_{e \times s}, \tag{14}$$

$$X = \begin{bmatrix} Q_{11} & Q_{12} & Q_{13} & \dots & Q_{1s} \\ Q_{21} & Q_{22} & Q_{13} & \dots & Q_{2s} \\ \vdots & \vdots & \vdots & \ddots & \vdots \\ Q_{e1} & Q_{e2} & Q_{e3} & \dots & Q_{es} \end{bmatrix}_{e \times s} \tag{15}$$

Now, the linearized elemental heat generation vector $\bar{Q}^{\emptyset}$, is obtained by taking the weighted average of these snapshots:

$$\bar{Q}^{\emptyset} = \sum_{i=1}^{s} w_i q_i, \tag{16}$$

where, w_i denote the weights applied to obtain the linearized elemental heat generation load vector. Note that, the ANSYS FEM simulator [13] automatically distributes the elemental load values onto n finite element nodes to create the nodal load vector $\bar{Q}$ for the model (3). Section 5 details the construction of optimal load vector.

5 Results

For this case-study we use 15 load-vector snapshots and weight them in different ways as follows:
1. $w_1 = 0.35$, $w_2 = 0.25$, $w_3 = 0.25$, $w_4 = 0.1$, $w_5 = 0.05$, w_6 to $w_{15} = 0$ (first snapshots densely weighted).
2. $w_{11} = 0.1$, $w_{12} = 0.1$, $w_{13} = 0.25$, $w_{14} = 0.25$, $w_{15} = 0.3$, w_1 to $w_{10} = 0$ (last snapshots densely weighted).
3. w_1 to $w_{15} = 1$ (equal weight distribution).
The linearized elemental heat generation vector $\bar{Q}^{\emptyset}$ is obtained according to (16) and the linearized nodal load vector is correspondingly created by ANSYS.

Figure 3 shows the study carried out for the selection of optimal weights. The snapshots are distributed into three groups having five snapshots each; separated by the dashed lines. As expected, within the time domain in which we weigh the snapshots densely, the match between the full and the reduced model is better.

Based on this outcome, optimal weights are selected as follows:
$w_1 = 0.15$, $w_2 = 0.12$, $w_3 = 0.08$, $w_4 = 0.08$, $w_5 = 0.05$, $w_6 = 0.05$, $w_7 = 0.08$, $w_8 = 0.08$, $w_9 = 0.1$, $w_{10} = 0.05$, $w_{11} = 0.05$, $w_{12} = 0.05$, $w_{13} = 0.05$, $w_{14} = 0.01$, $w_{15} = 0.01$.

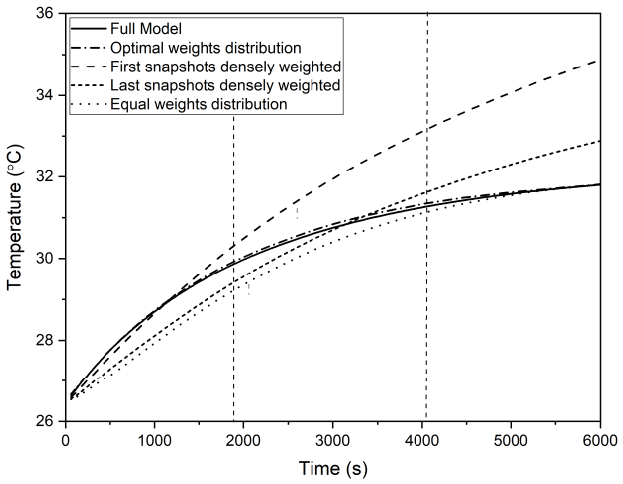

Fig. 3 Temperature result comparison between full and reduced model at the bottom surface of TEG with different weighing of snapshots.

Figure 4 shows the result comparison between the full model of order 127,944 and reduced model of order 30., with optimal weights selection. An excellent match is obtained.

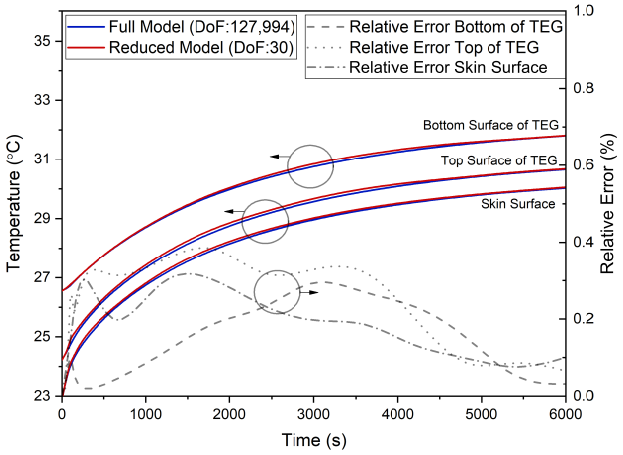

Fig. 4 Result comparison between full model with nonlinear-input and reduced linearized model with optimal distribution of snapshots, at the top and bottom surfaces of TEG and skin surface.

6 Conclusion and Outlook

In this work, we studied the problem of constructing a reduced order model for first order dynamical system with nonlinear-input. It mathematically describes a thermal model of TEG embedded in human tissue structure. We presented the result comparison between the full model and reduced linearized model during the transient simulation. The approach presented here, allows the direct implementation of model order reduction for large-scale thermal models with nonlinear-input. The costs for evaluating the nonlinear input term is reduced by snapshot-based linearization.
Note that, the implemented approach works well for the step input function (applicable to current case-study), might however, fail for other types of input functions. A remedy might be to apply the Proper Orthogonal Decomposition (POD) approach for constructing a reduced order model. From our preliminary computations, it turns out that, only two POD modes are enough to obtain the good approximation of the full-scale model.

References

1. Kerley, R., Huang, X., Ha, D.S.: Energy Harvesting from the Human Body and Powering up Implant Devices. In: Nano Devices and Circuit Techniques for Low-Energy Applications and Energy Harvesting, pp. 147-180, Springer Netherlands, Dordrecht (2016)
2. Mitcheson, P. D., Yeatman, E. M., Rao, G. K., Holmes, A. S., Green, T. C.: Energy Harvesting From Human and Machine Motion for Wireless Electronic Devices. Proceedings of the IEEE, **96**, 1457–1486 (2008)
3. Tsui, C. Y., Li, X., Ki, W. H.: Energy Harvesting and Power Delivery for Implantable Medical Devices. Foundations and Trends®in Electronics Design Automation, **7**, 179–246 (2013)
4. Lu, B. W., Chen, Y., Ou, D. P., Chen, H., Diao, L. W., Zhang, W., Zheng, J., Ma W. G., Sun, L. Z., Feng, X.: Ultra-flexible Piezoelectric Devices Integrated with Heart to Harvest the Biomechanical Energy. Sci. Rep. 5, 16065, (2015)
5. Chen, A.: Thermal Energy Harvesting with Thermoelectrics for Self-powered Sensors: With applications to Implantable Medical Devices, Body Sensor Networks and Aging in Place. Ph.D. thesis, University of California, Berkeley (2011).
6. Parsons, K.: Human Thermal Environments. In: A book for thermal environment, Taylor&Francis, (2003)
7. Antoulas, A. C.: Approximation of Large-Scale Dynamical Systems. In: Society for Industrial and Applied Mathematics, (2005)
8. Bechtold, T., Rudnyi, E., Korvink, J. G.: Fast Simulation of Electro-Thermal MEMS. In: Springer-Verlag Berlin Heidelberg, (2007)
9. Jadhav, O., Yuan, C. D., Hohlfeld, D., Bechtold, T.: Design of a thermoelectric generator for electrical active implants. MikroSystemTechnik Congress, 1–4 October (2017)
10. Pennes, H. H.: Analysis of tissue and arterial blood temperatures in the resting human forearm. Journal of applied physiology, **1**, 93–122 (1948)
11. Rother, S., Beitelschmidt, M.: Load Snapshot Decomposition to Consider Heat Radiation in Thermal Model Order Reduction. 9th Vienna International Conference on Mathematical Modelling, **51**, 667–672 (2018)
12. Freund, R. W.: Krylov-subspace methods for reduced-order modeling in circuit simulation. Linear Algebra and its Applications, **415**, 406–425 (2006)
13. ANSYS: Academic Research Mechanical, Release 18.1, Help System, Coupled Field Analysis Guide. ANSYS, Inc.